IEEE Access
Multidisciplinary : Rapid Review : Open Access Journal

Received June 9, 2020, accepted July 9, 2020, date of publication July 13, 2020, date of current version July 23, 2020.

Digital Object Identifier 10.1109/ACCESS.2020.3008858

Super Twisting Fractional Order Energy Management Control for a Smart University System Integrated DC Micro-Grid

YASSER MOHAMMED ALHARBI[1], AHMAD AZIZ AL ALAHMADI[1], NASIM ULLAH[1], (Member, IEEE), HABTI ABEIDA[1], MOHAMED S. SOLIMAN[1,2], (Senior Member, IEEE), AND YAHYA SALAMEH HASSAN KHRAISAT[1,3]

[1]Department of Electrical Engineering, Taif University, Ta'if 26571, Saudi Arabia
[2]Department of Electrical Engineering, Faculty of Energy Engineering, Aswan University, Aswan 81528, Egypt
[3]Department of Electrical and Electronics Engineering, Al-Balqa' Applied University, Amman 19117, Jordan

Corresponding author: Nasim Ullah (nasimullah@tu.edu.sa)

This work was supported by the Research Groups Program funded by Deanship of Scientific Research, Taif University, Ministry of Education, Saudi Arabia, under Grant 1-440-6140.

ABSTRACT This paper designs an intelligent energy management control for a stand alone smart DC-micro-grid using super twisting fractional order method. Based on mathematical model of the micro-grid, controllers are derived for the source side converters such as photovoltaic (PV),wind, AC grid and battery management system, and load side converters. Based on the available measured input and consumed output power, an intelligent energy management algorithm decides the appropriate mode of operation for the source and load side converters controller. All DC loads connected to the micro-grid are treated as essential loads and no load shedding can be allowed by the energy management unit. The energy management unit prioritizes the renewable energy sources (PV and wind) in order to make the micro-grid as cost effective. The performance of the proposed control scheme is compared with the integer order controller and the system is simulated in MATLAB/SIMULINK environment for different test cases.

INDEX TERMS DC micro-grid, robust control, sliding mode control, fractional calculus, energy management.

I. INTRODUCTION

In order to meet the raising power demands of the communities around the globe, generation from traditional power sources is no more a viable choice due to the emission of green house gases and the environmental problems [1]. In order to minimize the emission of green house gases and to reduce environmental pollution, the bulk power is now generated from the clean renewable energy sources such as photo voltaic (PV), wind, sea waves and fuel cells. The renewable energy sources are either integrated together to form standalone micro-grids or the available power from such sources is transferred to the existing power grids [2], [3]. Due to stochastic nature of renewable energy sources, auxiliary power sources such as energy storage system must be integrated to the system as a backup power sources [3], [4]. Usually it is preferred to integrate different clean power sources such as PV, wind and fuel cells [5], [6], because the combination of several such power sources with stochastic nature may have a positive impact on the maximum capacity of the energy storage system [7]. The combination of battery and ultra capacitor is utilized as energy storage system when a fast response of the system is required to compensate the transients. [8], [9]. Such combination can extend the life time of the battery storage system, however where all connected loads are essential, then instead of ultra capacitor AC grid is utilized as a back power source [9]. The integration of all power sources with battery storage system forms a micro-grid. A micro-grid is further categorized as either direct current (DC) or alternating current (AC) or a combination of AC and DC types. In comparison to AC micro-grid, DC offers several advantages such as its simple structure, few parameters to control and ease of installation and integration [10], [11]. On the other hand, an AC micro-grid

The associate editor coordinating the review of this manuscript and approving it for publication was Nishant Unnikrishnan.

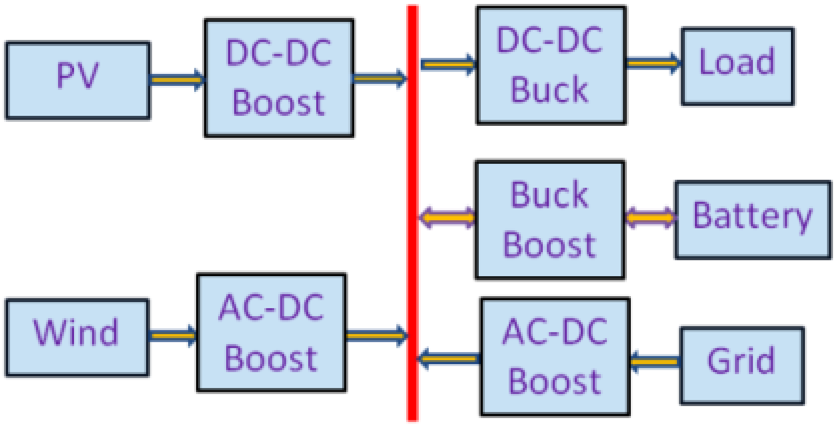

FIGURE 1. Block diagram of smart DC Micro-Grid.

requires additional parameters such as reactive power control and frequency synchronization, thus the control algorithm is computationally more complex [12], [13]. DC micro-grid can operate in several modes such as standalone, integrated with AC micro-grid or main AC grid. Due to the recent advances in power electronics switches, the standalone DC micro-grid can operate on maximum efficiency, however due to stochastic nature of the power sources, an additional energy management unit is required for the smooth operation and for the delivery of uninterruptible power to the loads. Several control methods integrated with energy management units have been reported for AC micro-grids [13]–[17], however since the dynamics of AC and DC quantities are different so the reported methods cannot be utilized for the DC micro-grids. In a typical DC micro-grid configuration, the source and load converters are connected in parallel to each other and energy is supplied or consumed from the main voltage bus referred as DC link. The mathematical dynamics of the system are non linear and coupled. The stabilization of DC link voltage is required for stable operation of the DC micro-grids [18]. Since the system dynamics are coupled, so the stabilization of DC link voltage is a difficult task to achieve and it requires sophisticated control methods [19], [21]. Linear control methods are often easy to implement. In [19], [22], [23], linear controllers are reported for the DC link voltage stabilization problem. However the utilized dynamic models are linear in nature and thus the proposed linear controllers can regulate the DC link voltage in a small operating envelop. Apart from linear controllers, several robust controllers have been reported in the literature such as Robust $H\infty$ control technique in [24], adaptive droop control method in [25], nonlinear sliding mode control in [26], [27], feedback linearization method in [28] and Lyapunov based method in [29]. The literature reported in [24]–[29] offer several limitations such as lack of rigorous stability analysis in case of $H \infty$ method, poor performance of droop control based methods with several sources integrated together, chattering problem in sliding mode control method, small operating envelop in case of general linearization method. The Lyapunov based method showed promising performance, however the energy management unit is not reported in subject work. In [30], [31], centralized robust and optimal controllers are reported for stability issues in DC micro-grid, however the effects of communication link such as network delays and its failure have not investigated. In [32]–[38] several other nonlinear control methods have been proposed with energy management units but all the presented methods are integer order. Fractional order controllers offer additional advantages over integer order controllers such as high degree of freedom. robust behavior to the measurement noise and oscillations. Several fractional order controllers have been reported in the literature such as DC-DC converters feeding constant power loads [31], robust non integer controller applied to nonlinear dynamic system [38], [39] and fuzzy fractional controller to servo systems [40], [41].

Based on the above literature survey, this paper proposes a decentralized super twisting fractional order control integrated with energy management unit for the proposed DC micro-grid shown in Figure 1. The proposed fractional order controllers will serve as low-level control. The high level control is managed by the energy management unit which monitors the generated and consumed power and generate appropriate references for the low level control. Major contributions of this research work are as following.

1: According to the author,s best knowledge, fractional order controllers have never been exploited for a DC- micro-grid integrated with several stochastic sources and essential DC loads.

2: The proposed fractional order controllers offer minimum oscillations in the DC link voltage, thus enhancing the stability of the system.

3: Large signal model of the DC micro-grid is utilized for controller formulation with power stage parameters uncertainty.

4:Global stability of the closed loop system is ensured using fractional order Lyapunov theorem.

5: In the reported back-stepping control methods for DC micro-grids, the inner loop current references are set by the outer voltage loops, while the proposed sliding surfaces offer flexibility in adjusting the reference currents from user input or from energy management unit in a convenient way.

The rest of the paper is organized as follows: Section II describes the system configuration of the DC micro-grid, mathematical modeling is performed in Section III,Controllers are derived in Section IV, the energy management unit is discussed in Section V, results are discussed in Section VI and finally the conclusion is made in Section VII.

II. SYSTEM DESCRIPTION

Figure 1 shows the block diagram of a smart DC Micro-Grid. The sources include solar PV, wind and main ac grid. Apart from the sources, a battery storage system is also interfaced to the main DC bus. All sources are interfaced to the DC link via DC-DC converters. The battery storage system is connected through a bi directional buck-boost converter. As shown in the block diagram, the loads are driven by the load side converters. All loads are assumed to be priority loads that may include lighting, fans, and laboratory test benches for students experimentation. The power management unit calculates the total generated and consumed power and based on it, the appropriate control modes are utilized. The specifications of the system are tabulated in the results and discussion section.

III. MATHEMATICAL MODELING

1. Source Side Converters: In this section, the mathematical models for source-side converters are presented. Based on the presented models, the controllers are derived using fractional calculus. Basic fractional mathematics is given in Appendix-I.

A. PV CONVERTER SYSTEM MODEL

The PV converter system connected to the DC bus is shown in Figure 2. A boost converter is used to integrate the solar power to the main DC bus. The mathematical model for PV converter system can be written as:

$$\frac{dV_{pv}}{dt} = \frac{I_{pv}}{C_p} - \frac{I_{L_{pv}}}{C_p} \tag{1}$$

$$\frac{dI_{L_{pv}}}{dt} = \frac{V_{pv}}{L_{pv}} - (1 - U_1)\frac{V_{dc}}{L_{pv}} + D_1 \tag{2}$$

$$\frac{dV_{dc}}{dt} = (1 - U_1)\frac{I_{L_{pv}}}{C_{dc}} - \frac{I_{o_{pv}}}{C_{dc}} + D_2 \tag{3}$$

where V_{pv} represents the PV input voltage, I_{pv} is the PV current,$I_{L_{pv}}$ represents inductor current, V_{dc} represents dc link voltage, L_{pv} represents the inductance and U_1 is the control signal. The terms D_1 and D_2 represent the uncertainty dynamics in the power stage parameters.

B. WIND CONVERTER SYSTEM MODEL

The wind converter system connected to the DC bus is shown in Figure 3. A rectifier is used to convert the alternating power

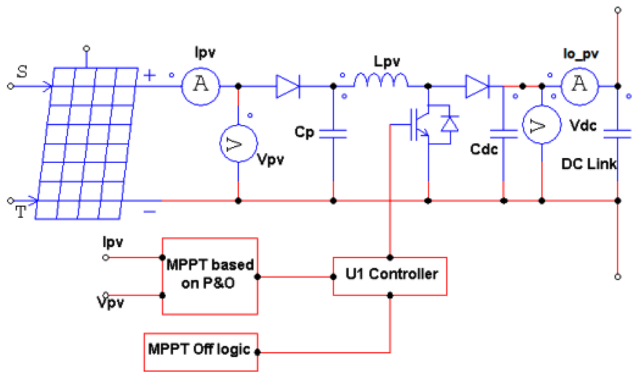

FIGURE 2. Block diagram of PV converter module.

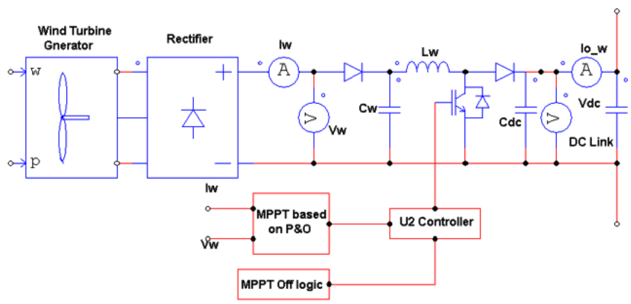

FIGURE 3. Block diagram of wind converter module.

to direct power and then a boost converter is used to integrate the wind power to the main DC bus. The mathematical model of the wind converter system is derived as following.

$$\frac{dV_w}{dt} = \frac{I_w}{C_w} - \frac{I_{L_w}}{C_w} \tag{4}$$

$$\frac{dI_{L_w}}{dt} = \frac{V_w}{L_w} - (1 - U_2)\frac{V_{dc}}{L_w} + D_3 \tag{5}$$

$$\frac{dV_{dc}}{dt} = (1 - U_2)\frac{I_{L_w}}{C_{dc}} - \frac{I_{o_w}}{C_{dc}} + D_4 \tag{6}$$

where V_w represents the wind rectified voltage input to the boost converter, I_w is the rectified wind current,I_{L_w} represents inductor current, V_{dc} represents dc link voltage, L_w represents the inductance and U_2 is the control signal. The terms D_3 and D_4 represent the uncertainty dynamics in the power stage parameters.

C. AC GRID CONVERTER SYSTEM MODEL

The AC grid converter system is similar to the wind converter system. A rectifier is used to convert the alternating power to direct power, then a boost converter is used to integrate the main AC grid into the DC bus. The mathematical model of the wind converter system is derived as follows:

$$\frac{dV_g}{dt} = \frac{I_g}{C_g} - \frac{I_{L_g}}{C_g} \tag{7}$$

$$\frac{dI_{L_g}}{dt} = \frac{V_g}{L_g} - (1 - U_3)\frac{V_{dc}}{L_g} + D_5 \tag{8}$$

$$\frac{dV_{dc}}{dt} = (1 - U_3)\frac{I_{L_g}}{C_{dc}} - \frac{I_{o_g}}{C_{dc}} + D_6 \tag{9}$$

where V_g represents the grid rectified voltage input to the grid boost converter, I_g is the rectified grid current,I_{L_g} represents inductor current, V_{dc} represents dc link voltage, L_g represents the inductance of the grid,s converter and U_3 is the control signal. The terms D_5 and D_6 represent the uncertainty dynamics in the power stage parameters. Here it is worth to mention that the supply of the grid power is assumed to be constant so no MPPT will be employed for the grid converter system.

D. BATTERY STORAGE CONVERTER SYSTEM MODEL

Block diagram of battery storage system is shown in Figure 4. A buck boost converter is used for the integration of battery storage system to the main DC bus of the micro-grid. Depending on the state of charge (SOC), source side power availability and load side power demand, battery storage system can work either in charging or discharging mode. In charging mode, power from the main bus is transferred to the batteries and,therefore,the converter works in buck mode. When power is supplied back to the micro-grid, the battery converter operates in boost mode. The mathematical model of the battery converter system is derived as following.

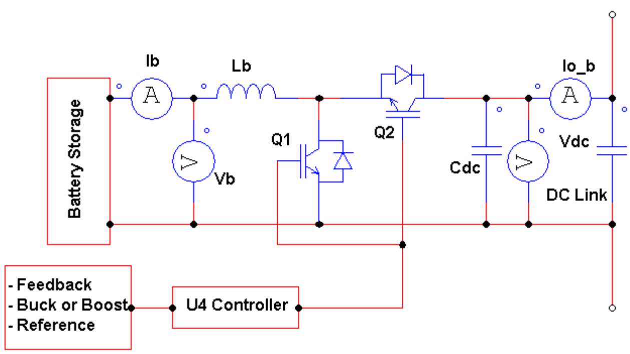

FIGURE 4. Battery storage converter module.

1. Boost mode: In boost mode, the reference battery current generated by the energy management system is positive. So the the boost mode is modeled as follows:

$$\frac{dI_b}{dt} = \frac{V_b}{L_b} - (1 - U_{Q1})\frac{V_{dc}}{L_b} + D_7 \tag{10}$$

$$\frac{dV_{dc}}{dt} = (1 - U_{Q1})\frac{I_b}{C_{dc}} - \frac{I_{o_b}}{C_{dc}} + D_8 \tag{11}$$

where V_b represents the battery voltage, I_b is the battery current, and U_{Q1} is the control signal. The terms D_7 and D_8 represent the uncertainty dynamics in the power stage parameters.

2. Buck mode: In buck mode, the reference battery current generated by the energy management system is negative. So the buck mode is modeled as follows:

$$\frac{dI_b}{dt} = \frac{V_b}{L_b} - U_{Q2}\frac{V_{dc}}{L_b} + D_7 \tag{12}$$

$$\frac{dV_{dc}}{dt} = U_{Q2}\frac{I_b}{C_{dc}} - \frac{I_{o_b}}{C_{dc}} + D_8 \tag{13}$$

where U_{Q2} is the control signal in buck mode. The generalized model representing the buck and boost mode is expressed as follows:

$$\frac{dI_b}{dt} = \frac{V_b}{L_b} - U_4\frac{V_{dc}}{L_b} + D_7 \tag{14}$$

$$\frac{dV_{dc}}{dt} = U_4\frac{I_b}{C_{dc}} - \frac{I_{o_b}}{C_{dc}} + D_8 \tag{15}$$

where $U_4 = sw(1 - U_{Q1}) + (1 - sw)U_{Q2}$. When $sw = 0$ the buck mode controller U_{Q2} is activated and with $sw = 1$, the boost mode control U_{Q1} is active.

E. SOURCE SIDE CONVERTERS GENRALIZED MODEL

In order to avoid the derivation of controllers for each source side converter, the mathematical models presented in Eqs.(1)-(9) and Eqs (14)-(15) are expressed in generalized form as following:

$$\frac{dV_J}{dt} = \frac{I_J}{C_K} - \frac{I_{L_J}}{C_K} \tag{16}$$

$$\frac{dI_{L_J}}{dt} = \frac{V_J}{L_J} - (1 - U_i)\frac{V_{dc}}{L_J} + D_i \tag{17}$$

$$\frac{dV_{dc}}{dt} = (1 - U_i)\frac{I_{L_J}}{C_{dc}} - \frac{I_{o_J}}{C_{dc}} + D_{i+1} \tag{18}$$

In Eqs. (16)-(18), the subscript J represents the sub subscripts pv, $wind$, g and b, while subscript K represents the sub subscripts P, w and g. The term i is 1 for pv, 2 for w, 3 for g and 4 for subscript b.

2. Load Side Converters: As shown in Figure 1, DC priority loads are connected through parallel DC/DC buck converters. Parallel converters are used to divide the load and reduce the stress on each converter. Moreover the DC loads are constant power loads.

The generalized model for p buck converters connected in parallel is expressed as following.

$$\frac{dI_{Lp}}{dt} = \frac{U_p V_{dc}}{L_p} - \frac{V_{load_p}}{L_p} + D_{I_{Lp}} \tag{19}$$

$$\frac{dV_{load_p}}{dt} = \frac{I_{Lp}}{C_p} - \frac{V_{load_p}}{R_{Lp}C_p} + D_{V_{load_p}} \tag{20}$$

where $p = 1, 2, 3 - n$ which represents the number of buck converters, I_{Lp} represents inductor current, V_{load_p} is the load voltage, L_p represents the inductance, C_p represents the output capacitance and U_p is the generalized control law. $D_{I_{Lp}}$ represents the uncertainty in the current dynamics while $D_{V_{load_p}}$ is the uncertainty of voltage dynamics.

IV. CONTROL SYSTEM FORMULATION

In this section the control system is derived for both source and load side converters of the proposed micro-grid based on fractional order super twisting method. Before going into the detailed derivations, the super twisting control is briefly explained. Referring to [31], [42], the super twisting control system consists of two parts. The first part is called the equivalent control which is derived based on system nominal model. The second part is the switching control part that is

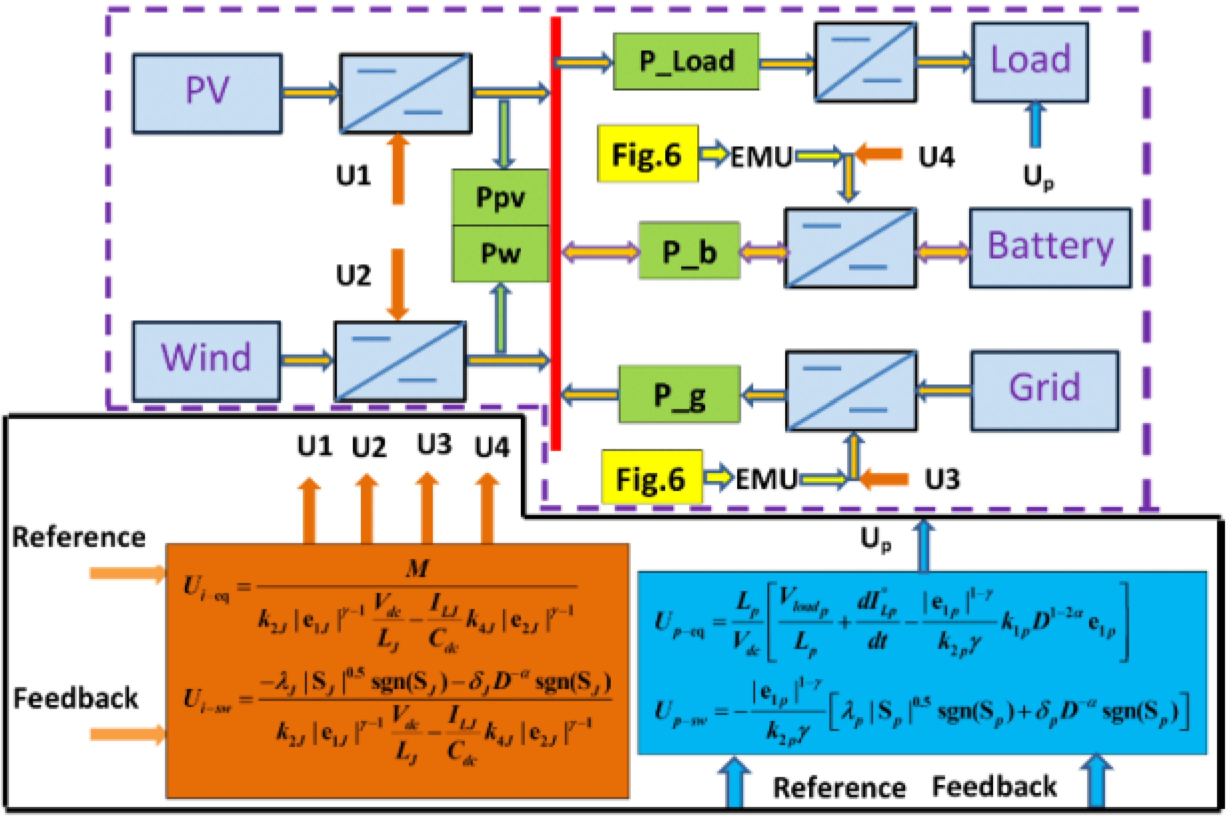

FIGURE 5. Control System block diagram.

based on the signum function and a nonlinear sliding surface. In comparison to the classical sliding mode control, the sliding surface is nonlinear in super twisting control system. As shown from Fig. 1-5, there are four source side and two load side converters, so the source side controllers $[U_1 - U_4]$ are generalized in the system model of Eq. 16-18 as U_i. Similarly the load side controllers are generalized as U_p given in Eq. 19-20. So U_i is derived for source side and U_p for load side converters. A simplified diagram explaining the the overall control and energy management unit of the micro-grid is shown in Fig. 5

1 Source side converters control: In this section the control law is derived based on the generic mathematical model presented in Eqs. (16)-(18). Eq. (16) is used to generate reference current I_{L_J} for pv, w and g while for the battery storage system, this reference current is generated by the energy management system. To derive the control law, let a Lyapunov function is expressed as $V_{J1} = 0.5\, e_J^2$. Where the error e_J and its first derivative are expressed as follows.

$$e_J = C_K(V_J - V_J^*) \quad (21)$$
$$\dot{e_J} = C_K(\dot{V_J} - \dot{V_J^*}) \quad (22)$$

Here V_J^* represents the reference voltage command.By combining Eq. (16) and (22), one obtains the following relation.

$$\dot{e_J} = (I_J - I_{L_J} - C_K\dot{V_J^*}) \quad (23)$$

The reference current I_{L_J} is calculated from Eq. (23) and it is expressed as follows:

$$I_{L_J^*} = -C_K\dot{V_J^*} + I_J + k_J e_J \quad (24)$$

By combining the first derivative of V_{J1} with Eq. (24), yields the following expression:

$$\dot{V_{J1}} = -k_J e_J^2 \quad (25)$$

where k_J represents the gain matrix and by choosing $k_J > 0$, Eq. (25) is always negative definite. The reference current for the battery storage system is generated by energy management system. $I_{L_J^*}$ represents virtual control law. To derive the actual control system U_i, fractional order sliding manifold is chosen in the light of the concepts presented in [31] as follows:

$$S_J = k_{1J}D^{-\alpha}e_{1J} + k_{2J}D^{\alpha}|e_{1J}|^{\gamma}Sgn(e_{1J}) + k_{3J}D^{-\alpha}e_{2J} + k_{4J}D^{\alpha}|e_{2J}|^{\gamma}Sgn(e_{2J}) \quad (26)$$

In Eq. (26), k_{1J}, k_{2J}, k_{3J} and k_{4J} represent the gain matrix. The above sliding surface is chosen based on the concepts presented in [31]. The main difference of the proposed sliding surface in comparison with [31] is highlighted as follows: **a.** The proposed sliding surface of Eq. (26) has different dynamics in terms of fractional integration and derivative. **b.** The proposed sliding surface of Eq. (26) is proposed for J number of variables. Moreover the error e_{1J} and e_{2J} represent the current and dc link voltage errors, respectively defined as follows:$e_{1J} = I_{L_J} - I^*_{L_J}$, $\dot{e}_{1J} = \dot{I}_{L_J} - \dot{I}^*_{L_J}$ and $e_{2J} = V_{dc} - V^*_{dc}$, $\dot{e}_{2J} = \dot{V}_{dc} - \dot{V}^*_{dc}$. By taking the first derivative of Eq. (26) with respect to time, one obtains the following relation:

$$\dot{S}_J = k_{1J}D^{1-\alpha}e_{1J} + k_{2J}D^{\alpha}\gamma|e_{1J}|^{\gamma-1}\dot{e}_{1J} + k_{3J}D^{1-\alpha}e_{2J} + k_{4J}D^{\alpha}\gamma|e_{2J}|^{\gamma-1}\dot{e}_{2J} \quad (27)$$

By combining Eqs. (17) and (18) with Eq. (27) and multiply $D^{-\alpha}$ to both hand sides of the resultant expression, we get the following relation:

$$D^{1-\alpha}S_J = k_{1J}D^{1-2\alpha}e_{1J} + k_{2J}\gamma|e_{1J}|^{\gamma-1}[\frac{V_J}{L_J} - (1-U_i)\frac{V_{dc}}{L_J} + D_i - \dot{I}^*_{L_J}] + k_{3J}D^{1-2\alpha}e_{2J} + k_{4J}\gamma|e_{2J}|^{\gamma-1}[(1-U_i)\frac{I_{L_J}}{C_{dc}} - \frac{I_{oJ}}{C_{dc}} + D_{i+1} - \dot{V}^*_{dc}] \quad (28)$$

After expanding Eq. (28) and separating the terms containing U_i, the resultant equation is expressed as follows:

$$D^{\bar{\alpha}}S_J = k_{1J}D^{1-2\alpha}e_{1J} + k_{2J}\gamma|e_{1J}|^{\gamma-1}[\frac{V_J}{L_J} - \frac{V_{dc}}{L_J} + D_i - \dot{I}^*_{L_J}] + k_{3J}D^{1-2\alpha}e_{2J} + k_{4J}\gamma|e_{2J}|^{\gamma-1}[\frac{I_{L_J}}{C_{dc}} - \frac{I_{oJ}}{C_{dc}} + D_{i+1} - \dot{V}^*_{dc}] + U_i[k_{2J}\gamma|e_{1J}|^{\gamma-1}\frac{V_{dc}}{L_J} - \frac{I_{L_J}}{C_{dc}}k_{4J}\gamma|e_{2J}|^{\gamma-1}] \quad (29)$$

In Eq. (29), the operator $D^{\bar{\alpha}}$ is equal to $D^{1-\alpha}$ and it represents a fractional order derivative term. Using Eq. (29), the control law U_i is simplified as follows:

$$U_i = \frac{M - \lambda_J|S_J|^{0.5}sgn(S_J) - \delta_J D^{-\alpha}sgn(S_J)}{[k_{2J}\gamma|e_{1J}|^{\gamma-1}\frac{V_{dc}}{L_J} - \frac{I_{L_J}}{C_{dc}}k_{4J}\gamma|e_{2J}|^{\gamma-1}]} \quad (30)$$

In Eq. (30), M is expressed as follows:

$$M = -k_{1J}D^{1-2\alpha}e_{1J} - k_{2J}\gamma|e_{1J}|^{\gamma-1}[\frac{V_J}{L_J} - \frac{V_{dc}}{L_J} - \dot{I}^*_{L_J}] - k_{3J}D^{1-2\alpha}e_{2J} - k_{4J}\gamma|e_{2J}|^{\gamma-1}[\frac{I_{L_J}}{C_{dc}} - \frac{I_{oJ}}{C_{dc}} - \dot{V}^*_{dc}] \quad (31)$$

In Eq. (31), λ_J and δ_J represent gain of super-twisting sliding mode reaching law.The stability proof is given in Appendix III.

2. Load converters control: The generalized state space model for the load side converters is derived in Eqs. (19) and (20). To derive the control law U_p, let a Lyapunov function is expressed as $V_p = 0.5\ e_p^2$. Therefore error e_p and its first derivative are expressed as follows:

$$e_p = C_p(V_{load_p} - V^*_{load_p}) \quad (32)$$

$$\dot{e_p} = C_p(\dot{V_{load_p}} - \dot{V^*_{load_p}}) \quad (33)$$

By combining Eq. (20) and (33), one obtains the following relation:

$$\dot{e_p} = (I_{Lp} - \frac{V_{load_p}}{R_{Lp}} + C_pD_{V_{load_p}} - C_p\dot{V^*_{load_p}}) \quad (34)$$

The reference current I_{Lp} is calculated from Eq. (34) and it is expressed as follows:

$$I^*_{Lp} = \frac{V_{load_p}}{R_{Lp}} + C_p\dot{V^*_{load_p}} - k_pe_p - y_psgn(e_p) \quad (35)$$

By combining the first derivative of V_p with Eq. (35) yields the following expression:

$$\dot{V_p} = -k_pe_p^2 - y_p|e_p| \quad (36)$$

where k_p and y_p represent the gain matrix and by choosing $k_p > 0$ and $y_p > D_{V_{loadp(max)}}$, Eq. (36) is always negative definite.

To derive the actual control law U_p, fractional order sliding manifold is chosen as follows:

$$S_p = k_{1p}D^{-\alpha}e_{1p} + k_{2p}D^{\alpha}|e_{1p}|^{\gamma}Sgn(e_{1p}) \quad (37)$$

In Eq. (37), k_{1p} and k_{2p} represent the gain matrix. Moreover, the error e_{1p} represents the current error defined as follows:$e_{1p} = I_{Lp} - I^*_{Lp}$ and $\dot{e}_{1p} = \dot{I}_{Lp} - \dot{I}^*_{Lp}$. By taking the first derivative of Eq. (37), one obtains the following relation:

$$\dot{S_p} = k_{1p}D^{1-\alpha}e_{1p} + k_{2p}D^{\alpha}\gamma|e_{1p}|^{\gamma-1}\dot{e}_{1p} \quad (38)$$

By combining Eq. (19) and $\dot{e}_{1p}$ with Eq. (38), and multiply $D^{-\alpha}$ to both hand sides of the resultant expression, we get the following relation:

$$D^{\bar{\alpha}}S_p = D^{1-\alpha}S_p = k_{1p}D^{1-2\alpha}e_{1p} + k_{2p}\gamma|e_{1p}|^{\gamma-1}[\frac{U_pV_{dc}}{L_p} - \frac{V_{load_p}}{L_p} + D_{I_{Lp}} - \dot{I}^*_{Lp}] \quad (39)$$

where the operator $D^{\bar{\alpha}}$ is equal to $D^{1-\alpha}$ and it represents a fractional order derivative term. Using Eq. (39), the control system U_p is simplified as following.

$$U_p = \frac{L_p}{V_{dc}}[\frac{V_{load_p}}{L_p} + \dot{I}^*_{Lp} - \frac{|e_{1p}|^{1-\gamma}}{k_{2p}\gamma}[+k_{1p}D^{1-2\alpha}e_{1p} + \lambda_p|S_p|^{0.5}sgn(S_p) + \delta_pD^{-\alpha}sgn(S_p)] \quad (40)$$

where λ_p and δ_p represent gain of super-twisting sliding mode reaching law. To prove the stability of the closed loop system, the Lyapunov function can be expressed expressed as: $V_{U_p} = 0.5S_p^2$. By utilizing the concepts presented in the stability proof of the source converters control section, it is very to show that $D^{\bar{\alpha}}S_p \leq 0$.

V. ENERGY MANAGEMENT UNIT

In this section the energy management algorithm is discussed briefly. The unit measures the input power available from the PV and wind sources. Similarly, the consumed power on the load side is also measured and then based on a power balance equation, the energy management algorithm is developed which is shown in Figure 6. Input sources such as PV and wind systems are utilized on priority to feed the loads. In the case of abundant power from input sources, the additional

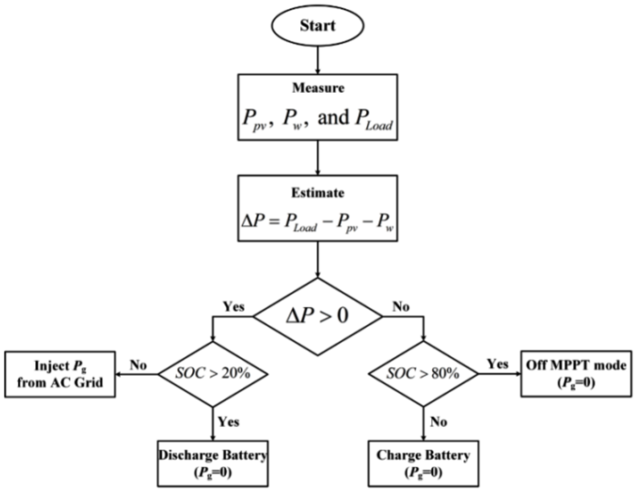

FIGURE 6. Energy management module.

power is used to charge the energy storage system. Usually in normal working conditions, no power is drawn from the AC grid. In a situation, when the power available from the PV, wind and battery storage system is not enough to drive the loads, then power from the AC grid is drawn to drive the loads. The power balance equation is expressed as follows:

$$P_w + P_{pv} + P_g = P_{Load} + P_{Battery} \tag{41}$$

When $P_{Load} - (P_w + P_{pv}) > 0$ then $P_g = 0$ and $P_{Battery}$ is supplied to the loads until the state of charge (SOC) is above 20 percent. When the SOC is less than 20 percent, then P_g is adjusted as per the load demand and $P_{Battery} = 0$. In the second case when $P_{Load} - (P_w + P_{pv}) < 0$ then $P_g = 0$ and the $P_{Battery}$ is absorbed from micro-grid to charge the battery storage system until the state of charge (SOC) is at maximum.The converters are operated on MPPT off mode when SOC > 80 percent.

VI. RESULTS AND DISCUSSION

In this section, the proposed controller is tested in simulation environment (MATLAB/Simulink) with the proposed DC micro-grid. All the parameters of the micro-grid subsystems and the controllers are tabulated in tables 1-4.

Overall the simulation results are focused on the verification of energy management unit (Figure 6) using the proposed control scheme.In the first case, fixed DC load of 8000 watts is connected through two load side converters to the DC voltage bus and state of charge (SOC) for battery storage system is initially set to 80 %. As shown in Figure 7a, the PV source is supplying fixed power of 2000 watts at a temperature of 25 degree Celsius and radiance of 600 watts/m2. The wind speed is varied between 8-13 m/s as shown in Fig. 7b and in response to it, the wind power is also varied between 4000 - 10000 watts which is shown in Figure 7c. Figure 8a shows the total power consumed by the load and it is around 8000 watts. The simulation results of the combined source power p_{dg}

TABLE 1. Parameters of PV system.

PV panels	
Number of series strings	18
Number of parallel strings	5
Open circuit voltage	$22V$
Short circuit current	$8.35A$
Voltage at MPP	$17.7V$
Voltage at MPP	$7.6A$

TABLE 2. Parameters of wind energy system.

Wind Turbine	
Turbine output (Watts)	15000
Air density (Kg/m3)	1.225
Base wind speed(m/s)	15
PMSG(Generator)	
Generator (VA)	17000
Stator phase resistance (ohm)	1.36
Armature inductance (H)	0.0125
Flux linkage(wb)	1.44
Inertia (kgm2)	0.1
Viscous damping(Nms)	0.0001
Pole pairs	4

TABLE 3. Parameters of battery storage system.

Lead acid battery	
Voltage (Volts)	261
Capacity (Ah)	208
Maximum Charge current(A)	25
Maximum discharge current(A)	40

TABLE 4. Converters and controllers parameters.

DC-DC converter parameters	
Inductance ($[L_J]$ $[L_p]$)(mH)	$([2.3, 5, 3.2, 4.1]$ $[4.4, 4.4])$
Capacitance ($[C_K]$ $[C_p]$ $[C_{dc}]$)(uF)	$([3, 3, 200]$ $[10, 10]$ $[100])$
Controller parameters	
Source side controller	
α	0.25
k_{1J}	$[10, 5, 1.5, 15]$
k_{2J}	$[5, 1.2, 10, 2.5]$
k_{3J}	$[12, 3.5, 7.5, 10]$
k_{4J}	$[12, 3.5, 7.5, 10]$
$-\lambda_J$	$[1.2, 1.2, 1.2, 1.2]$
$-\delta_J$	$[1.5, 1.5, 1.5, 1.5]$
Load side controller	
α	0.25
k_{1p}	$[1.5, 1.5]$
γ	0.45
k_{2p}	$[1.2, 1.2]$
$-\lambda_p$	$[0.15, 0.15]$
$-\delta_p$	$[0.25, 0.25]$

from both wind and PV sources are shown in Figure 8b. From the results presented, it is shown that p_{dg} increases from 6000-12000 watts during simulation time $t = [3 - 6]s$.Moreover since the consumed load power is fixed to 8000 watts (Figure 8a), while the combined source power p_{dg} is deficient in the time intervals $[1 - 3]s$, $[6 - 8]s$ and it is an excess amount for the time interval $[3 - 6]s$. With the above results presented, $\triangle P = P_{Load} - (P_w + P_{pv}) > 0$ in the time intervals $[0 - 3]s$, $[6 - 8]s$ and $\triangle P < 0$ for the time interval $[3-6]s$. As per the energy management algorithm of Figure 6, battery storage system will discharge to supply power to the

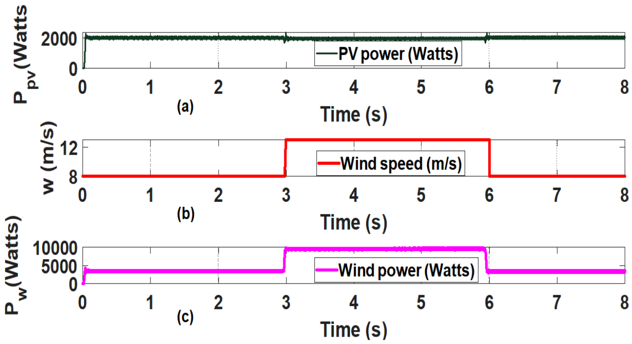

FIGURE 7. (a).PV power(Watts) (b). Wind speed (m/s) (c). Wind power (Watts).

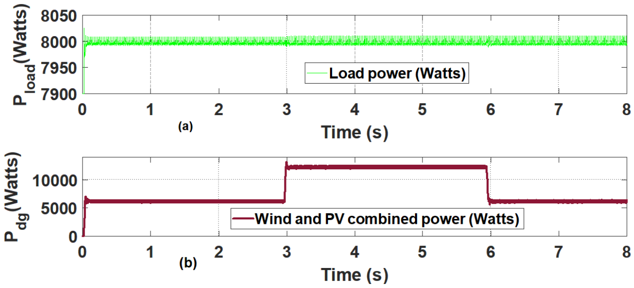

FIGURE 8. (a).Load power(Watts) (b). Wind and PV power (Watts).

micro-grid when $\triangle P > 0$ and $SOC > 20\%$, and it will charge if $\triangle P < 0$.

Figure 9a, 9b and 9c show the battery power, SOC and grid power simulations with the available combined source power p_{dg} of Figure 8b. As shown in Figure 9a, the battery supplies approximately 2000 watts to the micro-grid in the time intervals $[0-3]s$, $[6-8]s$ when $\triangle P > 0$ and $SOC > 20\%$, while in the time interval $[3-6]s$ the micro-grid source power p_{dg} is more than the load power,so the battery is charged and it absorbs 4000 watts from the micro-grid. Figure 9b shows the SOC simulations. From the presented results it is noted that the SOC decreases in the time intervals $[0-3]s$, $[6-8]s$ and it it increases in the time interval $[3-6]s$. Figure 9c shows the AC grid power supplied to the micro-grid. It is shown that $p_g = 0$ in all time intervals. The reason is very obvious because the $SOC > 20\%$, so no power is drawn from the AC grid by the micro-grid. Load power is shared between the two load converters. Load converter-1 consumes 4600 watts and converter-2 draws the remaining power of 3400 watts from the micro-grid. Figure 10a, 10b and 10c show the current sharing, load 1 and load 2 output voltage regulations simulation results. Since the load is fixed, so the simulation results with the proposed control schemes are included in the paper. From the presented results, it is clear that under the action of the proposed control scheme, load power is appropriately shared between the two converters,while the output voltages of each converter are accurately regulated to the reference value of 220 volts.

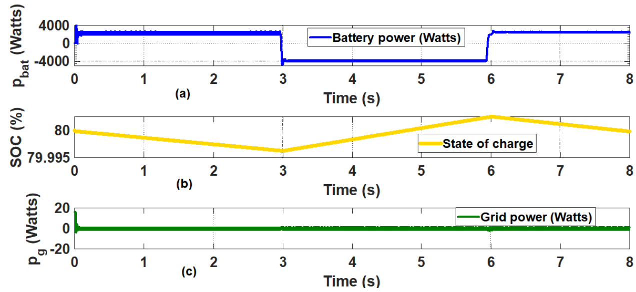

FIGURE 9. (a).Battery power(Watts) (b). SOC (%) c. Grid power (Watts).

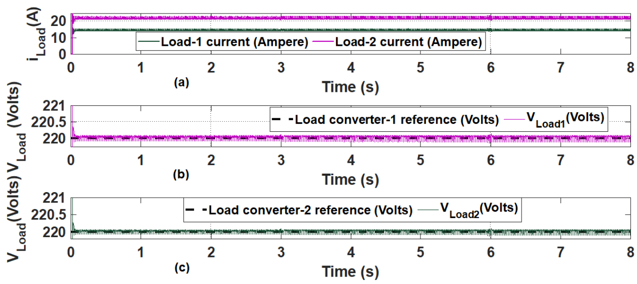

FIGURE 10. (a).Load sharing(Ampere) (b). Load-1 voltage c. Load-2 voltage).

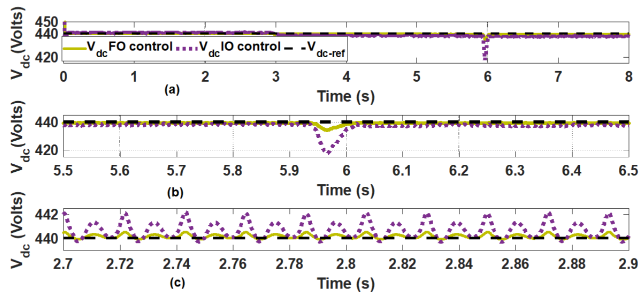

FIGURE 11. (a).Vdc regulation (b).Zoom in view1 c.Zoom in view2.

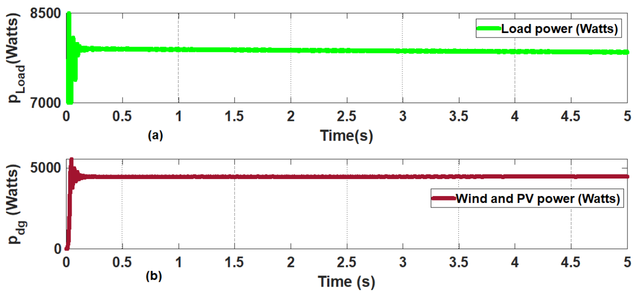

FIGURE 12. (a).Load power(Watts) (b). Wind and PV power (Watts).

It is also necessary to present a comparison of the proposed control system with its integer counter part. So an integer order controller is derived for the proposed micro-grid in Appendix-II. The stabilization of DC link voltage is very important because large fluctuations in it can cause system instabilities. Thus the results presented in Figure 11a, 11b and 11c give a fair performance comparison

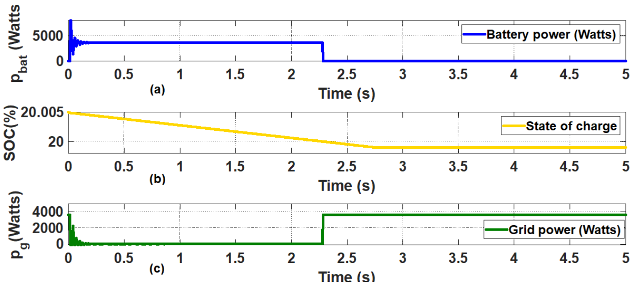

FIGURE 13. (a).Battery power(Watts) (b). SOC (%) c. Grid power (Watts).

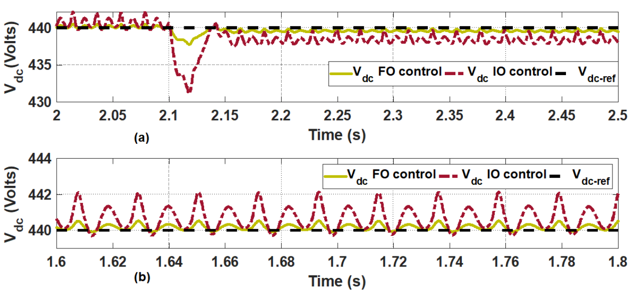

FIGURE 14. (a).Vdc regulation (b).Zoom in view1.

between the proposed and integer order control system given in Appendix-II. The load side converters are not considered as the loads are fixed. In the source side converters, the power stage parameters are subjected to uncertainty at time $t = 6s$. The uncertainty is introduced as following: $L_J \pm 15\% L_J$, $C_K \pm 15\% C_K$ and $C_{dc} \pm 15\% C_{dc}$, From the results presented in Figure 11, it is obvious that in the presence of the uncertainty and source side power variations, the proposed fractional order controller stabilizes the DC link voltage to its reference value (440 volts) with minimum oscillations and small steady state error.

The results presented in Figures 7-11 verify the proposed energy management system for all conditions when the state of charge of battery storage system, (SOC>20 %) and $p_g = 0$. In order to simulate the power injection mode from the main AC grid to the micro-grid, SOC of battery storage system is initially set to 20.005%. As shown in Fig. 12b, the combined source power p_{dg} is fixed at 4500 watts. Where out of 4500 watts, 2000 watts is contributed by PV sources as shown in Fig. 7a and the remaining 2500 watts is sourced from the wind power. Moreover fixed load of 8000 watts is connected to the micro-grid through two parallel load converters. The simulation results shown in Figure 12a and 12b show the available source power p_{dg} and load power. Now keeping in view this specific scenario, $\triangle P > 0$ and hence the battery storage system will discharge and supply additional power to drive the loads until SOC > 20%. Figure 13a, 13b and 13c show the simulation results of battery power, SOC and grid power. It is shown that in the time interval $t = [0 - 2.4]s$, the SOC>20% so the battery storage system is discharging and power is being supplied to the micro-grid. In the same interval, the AC grid power $p_g = 0$. But when the SOC < 20%, then the energy management disconnects the battery storage system and then power is supplied from the main AC grid. In order to compare the performance of the proposed controller with the integer order controller (Appendix-II), the source side converters are subject to the following uncertainty in its power stage parameters. $L_J \pm 25\% L_J$, $C_K \pm 10\% C_K$ and $C_{dc} \pm 15\% C_{dc}$. The uncertainty is introduced at time $t = 2.1s$. From the results presented in Figure 14a and 14b, it is obvious that in the presence of the uncertainty, the proposed fractional order controller stabilizes the DC link voltage to its reference value (440 volts) with minimum oscillations and small steady state error as compared to its integer order counter part controller.

VII. CONCLUSION

In this work, a generalized nonlinear model of a DC micro-grid converters system is developed to formulate the proposed controller.All DC loads connected to the micro-grid are treated as essential loads and no load-shedding can be allowed by the energy management unit. An energy management unit is utilized to activate the appropriate mode of the controllers based on the measured source and load powers. The energy management unit prioritizes the renewable energy sources (PV and wind) in order to make the micro-grid as cost effective with essential loads and no load-shedding scheme. The proposed controller is successfully implemented and the energy management algorithm is verified. Moreover the performance of the proposed fractional order controller is compared with the integer order controller (Appendix-II) under system parameters uncertainty. The proposed controller showed superior performance over the integer control scheme.

APPENDIX

APPENDIX-I

Basics of the fractional mathematics is explained here.

Definition 1: The Riemann–Liouville fractional order integration and derivative of a function $f(t)$are expressed as following [39]–[41].

$$ {}_{t_0}I_t^{\alpha} f(t) = D_t^{-\alpha} f(t) = \frac{1}{\Gamma(\alpha)} \int_{t_0}^{t} \frac{f(\tau)}{(t-\tau)^{1-\alpha}} d\tau \tag{42} $$

$$ {}_{t_0}D_t^{\alpha} f(t) = \frac{d^{\alpha}}{dt^{\alpha}} f(t) = \frac{1}{\Gamma(m-\alpha)} \frac{d^m}{dt^m} \int_{t_0}^{t} \frac{f(\tau)}{(t-\tau)^{\alpha-m+1}} d\tau \tag{43} $$

where $\Gamma(.)$ represents the gamma function,, $m \in N$ and $m-1 < \alpha \leq m$

Using Eq. (42) and Eq. (43) the following relation holds: ${}_{t_0}D_t^{\alpha}({}_{t_0}I_t^{\alpha} f(t)) = f(t)$

Definition 2: The Caputo fractional order derivative of a function $f(t)$ is given by [38], [39].

$$ {}_{t_0}D_t^{\alpha} f(t) = \begin{cases} \frac{1}{\Gamma(m-\alpha)} \int_{t_0}^{t} \frac{f^{(m)}(\tau)}{(t-\tau)^{\alpha-m+1}} d\tau; & m-1 < \alpha < m \\ \frac{d^m}{dt^m} f(t); , & \alpha = m \end{cases} \quad (44) $$

The following relation also holds true for Caputo definitions: ${}_{t_0}D_t^{\alpha}({}_{t_0}I_t^{\alpha} f(t)) = f(t)$. Rieman-Liouville and Caputo definitions are very much similar; the only difference lies in dealing with the initial conditions. In Rieman-Liouville definition, the initial conditions are non-integer while for Caputo definition they are of integer order.

APPENDIX-II

In this appendix the integer order controllers for source side converters are derived. Let an integer order sliding manifold is chosen as follows:

$$ S_J = k_{1J} \int e_{1J} + k_{2J}|e_{1J}|^{\gamma} Sgn(e_{1J}) + k_{3J} \int e_{2J} + k_{4J}|e_{2J}|^{\gamma} Sgn(e_{2J}) \quad (45) $$

By taking the first derivative of Eq. (45), one obtains the following relation.

$$ \dot{S}_J = k_{1J}e_{1J} + k_{2J}\gamma|e_{1J}|^{\gamma-1}\dot{e}_{1J} + k_{3J}e_{2J} + k_{4J}\gamma|e_{2J}|^{\gamma-1}\dot{e}_{2J} \quad (46) $$

By combining Eqs. (17) and (18) with Eq. (46), we get the following relation.

$$ \begin{aligned} \dot{S}_J &= k_{1J}e_{1J} + k_{2J}\gamma|e_{1J}|^{\gamma-1}[\frac{V_J}{L_J} - \frac{V_{dc}}{L_J} \\ &+ D_i - \dot{I}^*_{L_J}] + k_{3J}e_{2J} \\ &+ k_{4J}\gamma|e_{2J}|^{\gamma-1}[\frac{I_{L_J}}{C_{dc}} - \frac{I_{oJ}}{C_{dc}} + D_{i+1} - \dot{V}^*_{dc}] \\ &+ U_i[k_{2J}\gamma|e_{1J}|^{\gamma-1}\frac{V_{dc}}{L_J} - \frac{I_{L_J}}{C_{dc}} k_{4J}\gamma|e_{2J}|^{\gamma-1}] \end{aligned} \quad (47) $$

Using Eq. (47), the control system U_i is simplified as following.

$$ U_i = \frac{M - \lambda_J|S_J|^{0.5}sgn(S_J) - \delta_J \int sgn(S_J)}{[k_{2J}\gamma|e_{1J}|^{\gamma-1}\frac{V_{dc}}{L_J} - \frac{I_{L_J}}{C_{dc}}k_{4J}\gamma|e_{2J}|^{\gamma-1}]} \quad (48) $$

In Eq. (48), M is expressed as following

$$ \begin{aligned} M &= -k_{1J}e_{1J} - k_{2J}\gamma|e_{1J}|^{\gamma-1}[\frac{V_J}{L_J} - \frac{V_{dc}}{L_J} - \dot{I}^*_{L_J}] \\ &- k_{3J}e_{2J} - k_{4J}\gamma|e_{2J}|^{\gamma-1}[\frac{I_{L_J}}{C_{dc}} - \frac{I_{oJ}}{C_{dc}} - \dot{V}^*_{dc}] \end{aligned} \quad (49) $$

To prove the stability of the closed loop system, the Lyapunov function as expressed as: $V_{U_i} = 0.5S_J^2$ By taking first derivative of the Lyapunov function and by combining it with Eq. (47), (48) and (49), it is easy to prove that $\dot{V}_{U_i} \leq 0$

APPENDIX III

To prove the stability of the closed loop system, the Lyapunov function can be expressed as: $V_{U_i} = 0.5S_J^2$ By applying fractional operator $D^{\bar{\alpha}}$ to the Lyapunov function: V_{U_i} yields the following expression [39]–[41].

$$ D^{\bar{\alpha}}U_i \leq S_J D^{\bar{\alpha}}S_J + \sum_{l=1}^{\infty} \frac{\mathcal{T}(1+\bar{\alpha})}{\mathcal{T}(1+\bar{\alpha}-l)(1+l)} D^l S_J D^{\bar{\alpha}-l} S_J \quad (50) $$

Consider the following inequality:

$$ \sum_{l=1}^{\infty} \frac{\mathcal{T}(1+\bar{\alpha})}{\mathcal{T}(1+\bar{\alpha}-l)(1+l)} D^l S_J D^{\bar{\alpha}-l} S_J \leq \zeta(S_J) \quad (51) $$

By combining Eqs. (29), (30), (50) and (51), the simplified equation can be expressed as follows:

$$ \begin{aligned} D^{\bar{\alpha}}U_i \leq\ & S_J[-\lambda_J|S_J|^{0.5}sgn(S_J) - \delta_J D^{-\alpha}sgn(S_J) \\ & + k_{2J}\gamma|e_{1J}|^{\gamma-1}D_i + k_{4J}\gamma|e_{2J}|^{\gamma-1}D_{i+1}] + \zeta(S_J) \end{aligned} \quad (52) $$

Eq. (52) can be expressed as follows:

$$ \begin{aligned} D^{\bar{\alpha}}U_i \leq\ & -\lambda_J|S_J|^{0.5}|S_J| - \delta_J D^{-\alpha}|S_J| \\ & + k_{2J}\gamma|e_{1J}|^{\gamma-1}S_J D_i + k_{4J}\gamma|e_{2J}|^{\gamma-1}S_J D_{i+1} + \zeta(S_J) \end{aligned} \quad (53) $$

In Eq. (53), by choosing λ_J and δ_J such that the combined effect of the term $-\lambda_J|S_J|^{0.5}|S_J| - \delta_J D^{-\alpha}|S_J|$ is more negative than the remaining terms $k_{2J}\gamma|e_{1J}|^{\gamma-1}S_J D_i + k_{4J}\gamma|e_{2J}|^{\gamma-1}S_J D_{i+1} + \zeta(S_J)$, then the fractional derivative of the Lyapunov function $D^{\bar{\alpha}}U_i \leq 0$. The condition is valid for both positive and negative values of sliding surface S_J subject to the condition that the maximum limits of disturbance terms $|D_{i-max}|$ and $|D_{i+1-max}|$ are known. With the above analysis, the reaching condition is achieved i.e. $S_J = 0$, then by multiplying Eq. (26) by $D^{\alpha+1}$ the resultant expression can be written in the following form.

$$ k_{1J}D^1 e_{1J} + k_{3J}D^1 e_{2J} = -D^{2\alpha}D^1[k_{2J}|e_{1J}|^{\gamma}Sgn(e_{1J}) - k_{4J}|e_{2J}|^{\gamma}Sgn(e_{2J})] \quad (54) $$

In Eq. (54), D^1 represents integer order derivative so the expression $D^{2\alpha}D^1[k_{2J}|e_{1J}|^{\gamma}Sgn(e_{1J}) - k_{4J}|e_{2J}|^{\gamma}Sgn(e_{2J})] = D^{2\alpha}[k_{2J}\gamma|e_{1J}|^{\gamma-1}\dot{e}_{1J} - k_{4J}\gamma|e_{2J}|^{\gamma-1}\dot{e}_{2J}]$. By multiplying both hand sides of Eq. (54) by D^{-1}, the simplified equation is given as follows:

$$ k_{1J}e_{1J} + k_{3J}e_{2J} = -D^{2\alpha-1}[k_{2J}\gamma|e_{1J}|^{\gamma-1}\dot{e}_{1J} - k_{4J}\gamma|e_{2J}|^{\gamma-1}\dot{e}_{2J}] \quad (55) $$

In Eq. (55), the left hand side terms are equated as: $E_{surface} = k_{1J}e_{1J} + k_{3J}e_{2J}$. Moreover, the term $D^{2\alpha-1}$ represents the fractional integrator as long a $\alpha < 0.5$. With the condition specified on α, Eq. (55) is simplified as follows:

$$ E_{surface} = -D^{2\alpha-1}[k_{2J}\gamma|e_{1J}|^{\gamma-1}\dot{e}_{1J} - k_{4J}\gamma|e_{2J}|^{\gamma-1}\dot{e}_{2J}] \quad (56) $$

In Eq. (56), $D^{-\bar{\bar{\alpha}}} = D^{2\alpha-1}$ as long as $\alpha < 0.5$.

Lemma 1:. Fractional integral of a fractional derivative of a function $f(t)$ is expressed as following [39]–[41]:

$$_aD_t^{-\alpha}\,{}_aD_t^{\alpha}f(t) = f(t) - \sum_{n}^{m}[{}_aD_t^{\alpha-n}f(t)]_{t=a}\frac{[t-a]^{\alpha-n}}{\tau[\alpha-n+1]} \tag{57}$$

where τ represents gamma function.

Lemma 2:. Fractional integral of a function $f(t)$ is upper bounded such that following condition is true. [39]–[41]:

$$||{}_aD_t^{-\alpha}f(t)||_\rho \leq \psi_J||f(t)||_\rho;\ [1 \leq \psi_J \leq \infty;\ 1 \leq \rho \leq \infty] \tag{58}$$

All parameters of Eq. (57) and (58) are defined in [39]–[41]. *Lemma 1* is applied to the left hand side expression, while *Lemma 2* is applied to the right hand expression of Eq. (56). Mathematically the expression $E_{surface} = D^{-\alpha}D^{\alpha}E_{surface}$ is valid. Therefore the application of *Lemma 1* to the above expression yields the following relations.

$$D^{-\alpha}D^{\alpha}E_{surface} = E_{surface} - [{}_{t_r}D_t^{\alpha-1}E_{surface}]_{t=t_r}\frac{(t-t_r)^{\alpha-1}}{\Gamma(\alpha)} \tag{59}$$

From Eq. (59), when $t = t_r$ then $D^{-\alpha}D^{\alpha}E_{surface} = E_{surface}$. The expression $E_{surface} = D^{-2}D^2\ E_{surface}$ is also mathematically valid. So the application of *Lemma 1* to the above expression yields the following relation.

$$D^{-2}D^2E_{surface} = E_{surface}(t) - [{}_{t_r}D_t^{2-1}E_{surface}]_{t=t_r}\frac{(t-t_r)^{2-1}}{2} - E_{surface}(t_r) \tag{60}$$

Therefore application of *Lemma 2* to the right hand terms of Eq. (56), yields the following relation:

$$-D^{2\alpha-1}[k_{2J}\gamma|e_{1J}|^{\gamma-1}\dot{e}_{1J} - k_{4J}\gamma|e_{2J}|^{\gamma-1}\dot{e}_{2J}] = -\psi_J[k_{2J}\gamma|e_{1J}|^{\gamma-1}\dot{e}_{1J} - k_{4J}\gamma|e_{2J}|^{\gamma-1}\dot{e}_{2J}] \tag{61}$$

By combining the terms in left hand side of Eq. (60) and (61), one obtains the following expression:

$$||E_{surface}(t) - [{}_{t_r}D_t^{2-1}E_{surface}]_{t=t_r}\frac{(t-t_r)^{2-1}}{2}|| - ||E_{surface}(t_r)|| \leq -||\psi_J[k_{2J}\gamma|e_{1J}|^{\gamma-1}\dot{e}_{1J} - k_{4J}\gamma|e_{2J}|^{\gamma-1}\dot{e}_{2J}]|| \tag{62}$$

In Eq. (62), by replacing $t = t_{S_J}$, the error terms e_{1J} and e_{2J} are zero. So the right hand side term and $E_{surface}(t)$ are equal to zero. So the remaining expression is written as follows:

$$t_r \leq t_{S_j} - \frac{2E_{surface}(t_r)}{\dot{E}_{surface}(t_r)} \tag{63}$$

Eq. (63) shows that the convergence time of the proposed controller is finite.

REFERENCES

[1] S. R. Bull, "Renewable energy today and tomorrow," *Proc. IEEE*, vol. 89, no. 8, pp. 1216–1226, Aug. 2001.

[2] R. H. Lasseter and P. Paigi, "Microgrid: A conceptual solution," in *Proc. IEEE 35th Annu. Power Electron. Spec. Conf.*, vol. 6, Jun. 2004, pp. 4285–4290.

[3] C. L. Benson and C. L. Magee, "On improvement rates for renewable energy technologies: Solar PV, wind turbines, capacitors, and batteries," *Renew. Energy*, vol. 68, pp. 745–751, Aug. 2014.

[4] A. Bari, J. Jiang, W. Saad, and A. Jaekel, "Challenges in the smart grid applications: An overview," *Int. J. Distrib. Sensor Netw.*, vol. 10, no. 2, Feb. 2014, Art. no. 974682.

[5] A. C. Luna, N. L. Diaz, M. Graells, J. C. Vasquez, and J. M. Guerrero, "Mixed-integer-linear-programming-based energy management system for hybrid PV-wind-battery microgrids: Modeling, design, and experimental verification," *IEEE Trans. Power Electron.*, vol. 32, no. 4, pp. 2769–2783, Apr. 2017.

[6] V. Khare, S. Nema, and P. Baredar, "Solar–wind hybrid renewable energy system: A review," *Renew. Sustain. Energy Rev.*, vol. 58, pp. 23–33, May 2016.

[7] R. Atia and N. Yamada, "Sizing and analysis of renewable energy and battery systems in residential microgrids," *IEEE Trans. Smart Grid*, vol. 7, no. 3, pp. 1204–1213, May 2016.

[8] W. Jing, C. Hung Lai, S. H. W. Wong, and M. L. D. Wong, "Battery-supercapacitor hybrid energy storage system in standalone DC microgrids: Areview," *IET Renew. Power Gener.*, vol. 11, no. 4, pp. 461–469, Mar. 2017.

[9] R. A. Dougal, S. Liu, and R. E. White, "Power and life extension of battery-ultracapacitor hybrids," *IEEE Trans. Compon. Packag. Technol.*, vol. 25, no. 1, pp. 120–131, Mar. 2002.

[10] H. Kakigano, M. Nomura, and T. Ise, "Loss evaluation of DC distribution for residential houses compared with AC system," in *Proc. Int. Power Electron. Conf. (ECCE ASIA)*, Jun. 2010, pp. 6–480.

[11] H. Lotfi and A. Khodaei, "AC versus DC microgrid planning," *IEEE Trans. Smart Grid*, vol. 8, no. 1, pp. 296–304, Jan. 2017.

[12] A. T. Elsayed, A. A. Mohamed, and O. A. Mohammed, "DC microgrids and distribution systems: An overview," *Electr. Power Syst. Res.*, vol. 119, pp. 407–417, Feb. 2015.

[13] J. Rocabert, A. Luna, F. Blaabjerg, and P. Rodríguez, "Control of power converters in AC microgrids," *IEEE Trans. Power Electron.*, vol. 27, no. 11, pp. 4734–4749, Nov. 2012.

[14] J. Kim, J. M. Guerrero, P. Rodriguez, R. Teodorescu, and K. Nam, "Mode adaptive droop control with virtual output impedances for an inverter-based flexible AC microgrid," *IEEE Trans. Power Electron.*, vol. 26, no. 3, pp. 689–701, Mar. 2011.

[15] H. Han, X. Hou, J. Yang, J. Wu, M. Su, and J. M. Guerrero, "Review of power sharing control strategies for islanding operation of AC microgrids," *IEEE Trans. Smart Grid*, vol. 7, no. 1, pp. 200–215, Jan. 2016.

[16] H. Cai, G. Hu, F. L. Lewis, and A. Davoudi, "A distributed feedforward approach to cooperative control of AC microgrids," *IEEE Trans. Power Syst.*, vol. 31, no. 5, pp. 4057–4067, Sep. 2016.

[17] J. M. Guerrero, J. C. Vasquez, J. Matas, L. G. de Vicuna, and M. Castilla, "Hierarchical control of droop-controlled AC and DC microgrids—A general approach toward standardization," *IEEE Trans. Ind. Electron.*, vol. 58, no. 1, pp. 158–172, Jan. 2011.

[18] D. Chen and L. Xu, "Autonomous DC voltage control of a DC microgrid with multiple slack terminals," *IEEE Trans. Power Syst.*, vol. 27, no. 4, pp. 1897–1905, Nov. 2012.

[19] H. Kakigano, Y. Miura, and T. Ise, "Distribution voltage control for DC microgrids using fuzzy control and gain-scheduling technique," *IEEE Trans. Power Electron.*, vol. 28, no. 5, pp. 2246–2258, May 2013.

[20] S. Anand, B. G. Fernandes, and J. M. Guerrero, "Distributed control to ensure proportional load sharing and improve voltage regulation in low voltage DC microgrids," *Fuel*, vol. 4, no. 3, pp. 1–33, 2013.

[21] A. Tani, M. Baïlo Camara, and B. Dakyo, "Energy management in the decentralized generation systems based on renewable energy—Ultracapacitors and battery to compensate the wind/load power fluctuations," *IEEE Trans. Ind. Appl.*, vol. 51, no. 2, pp. 1817–1827, May/Apr. 2015.

[22] M. Babazadeh and H. Karimi, "A robust two-degree-of-freedom control strategy for an islanded microgrid," *IEEE Trans. Power Del.*, vol. 28, no. 3, pp. 1339–1347, Jul. 2013.

[23] M. Kumar, S. C. Srivastava, and S. N. Singh, "Control strategies of a DC microgrid for grid connected and islanded operations," *IEEE Trans. Smart Grid*, vol. 6, no. 4, pp. 1588–1601, Jul. 2015.

[24] Y. A.-R.-I. Mohamed, H. H. Zeineldin, M. M. A. Salama, and R. Seethapathy, "Seamless formation and robust control of distributed generation microgrids via direct voltage control and optimized dynamic power sharing," *IEEE Trans. Power Electron.*, vol. 27, no. 3, pp. 1283–1294, Mar. 2012.

[25] X. Lu, J. M. Guerrero, K. Sun, and J. C. Vasquez, "An improved droop control method for dc microgrids based on low bandwidth communication with DC bus voltage restoration and enhanced current sharing accuracy," *IEEE Trans. Power Electron.*, vol. 29, no. 4, pp. 1800–1812, Apr. 2014.

[26] S. Singh, D. Fulwani, and V. Kumar, "Robust sliding-mode control of DC/DC boost converter feeding a constant power load," *IET Power Electron.*, vol. 8, no. 7, pp. 1230–1237, Jul. 2015.

[27] M. D. Cook, G. G. Parker, R. D. Robinett, and W. W. Weaver, "Decentralized mode-adaptive guidance and control for DC microgrid," *IEEE Trans. Power Del.*, vol. 32, no. 1, pp. 263–271, Feb. 2017.

[28] M. Cupelli, M. Moghimi, A. Riccobono, and A. Monti, "A comparison between synergetic control and feedback linearization for stabilizing MVDC microgrids with constant power load," in *Proc. Innov. Smart Grid Technol. Conf. Eur. (ISGT-Eur.)*, Oct. 2014, pp. 1–6.

[29] A. Iovine, M. J. Carrizosa, G. Damm, and P. Alou, "Nonlinear control for DC microgrids enabling efficient renewable power integration and ancillary services for AC grids," *IEEE Trans. Power Syst.*, vol. 34, no. 6, pp. 5136–5146, Nov. 2019.

[30] F. Ornelas-Tellez, J. J. Rico-Melgoza, E. Espinosa-Juarez, and E. N. Sanchez, "Optimal and robust control in DC microgrids," *IEEE Trans. Smart Grid*, vol. 9, no. 6, pp. 5543–5553, Nov. 2018.

[31] NasimUllah, M. Asghar, A. Khattak, and M. M. Rafiq, "Comparison of integer and fractional order robust controllers for DC/DC converter feeding constant power load in a DC microgrid," *Sustain. Energy, Grids Netw.*, vol. 12, Dec. 2017, pp. 1–9.

[32] T. K. Roy, M. A. Mahmud, A. M. T. Oo, M. E. Haque, K. M. Muttaqi, and N. Mendis, "Nonlinear adaptive backstepping controller design for islanded DC microgrids," *IEEE Trans. Ind. Appl.*, vol. 54, no. 3, pp. 2857–2873, May 2018.

[33] J. Hu, Y. Shan, Y. Xu, and J. M. Guerrero, "A coordinated control of hybrid AC/DC microgrids with PV-wind-battery under variable generation and load conditions," *Int. J. Electr. Power Energy Syst.*, vol. 104, pp. 583–592, Jan. 2019.

[34] M. A. Abdullah, A. H. M. Yatim, C. W. Tan, and R. Saidur, "A review of maximum power point tracking algorithms for wind energy systems," *Renew. Sustain. Energy Rev.*, vol. 16, no. 5, pp. 3220–3227, Jun. 2012.

[35] Naghmash, H. Armghan, I. Ahmad, A. Armghan, S. Khan, and M. Arsalan, "Backstepping based non-linear control for maximum power point tracking in photovoltaic system," *Sol. Energy*, vol. 159, pp. 134–141, Jan. 2018.

[36] A. Tahri, H. E. Fadil, F. Giri, and F. Z. Chaoui, "Nonlinear control and observation of a boost converter associated with a fuel-cell source in presence of model uncertainty," *IFAC Proc. Volumes*, vol. 47, no. 3, pp. 575–580, 2014.

[37] N. R. Tummuru, M. K. Mishra, and S. Srinivas, "Dynamic energy management of renewable grid integrated hybrid energy storage system," *IEEE Trans. Ind. Electron.*, vol. 62, no. 12, pp. 7728–7737, Dec. 2015.

[38] A. Rosa, M. Silva, M. Campos, R. Santana, W. Rodrigues, L. Morais, and S. I. Seleme, Jr., "SHIL and DHIL simulations of nonlinear control methods applied for power converters using embedded systems," *Electronics*, vol. 7, no. 10, p. 241, Oct. 2018.

[39] S. Dadras and H. R. Momeni, "Fractional terminal sliding mode control design for a class of dynamical systems with uncertainty," *Commun. Nonlinear Sci. Numer. Simul.*, vol. 17, no. 1, pp. 367–377, Jan. 2012.

[40] N. Ullah, W. Shaoping, M. I. Khattak, and M. Shafi, "Fractional order adaptive fuzzy sliding mode controller for a position servo system subjected to aerodynamic loading and nonlinearities," *Aerosp. Sci. Technol.*, vol. 43, pp. 381–387, Jun. 2015.

[41] N. Ullah, S. Han, and M. Khattak, "Adaptive fuzzy fractional-order sliding mode controller for a class of dynamical systems with uncertainty," *Trans. Inst. Meas. Control*, vol. 38, no. 4, pp. 402–413, Apr. 2016.

[42] I. Sami, S. Ullah, Z. Ali, N. Ullah, and J.-S. Ro, "A super twisting fractional order terminal sliding mode control for DFIG-based wind energy conversion system," *Energies*, vol. 13, no. 9, p. 2158, May 2020.

YASSER MOHAMMED ALHARBI received the Ph.D. degree in electrical engineering from Curtin University, Australia. He is currently an Assistant Professor with the Department of Electrical Engineering, Taif University, Saudi Arabia. His research interests include renewable energy systems, power system stability, power electronics, power quality, and system simulation.

AHMAD AZIZ AL ALAHMADI received the Ph.D. degree in nano-electronic devices from the School of Engineering, Ohio University, Athens, OH, USA. Since July 2017, he has been the Vice Dean of the Faculty of Engineering, Taif University, Saudi Arabia. He is currently an Associate Professor with the Department of Electrical Engineering, Faculty of Engineering, Taif University. His research interests include control systems and nano-electronic devices.

NASIM ULLAH (Member, IEEE) received the Ph.D. degree in mechatronic engineering from Beihang University, Beijing, China, in 2013. From September 2006 to 2010, he was a Senior Design Engineer with IICS, Pakistan. He is currently working as an Associate Professor of electrical engineering with Taif University, Saudi Arabia. His research interests include renewable energy, flight control systems, integer and fractional order modeling of dynamic systems, integer/fractional order adaptive robust control methods, fuzzy/NN, hydraulic and electrical servos, and epidemic and vaccination control strategies.

HABTI ABEIDA received the B.Sc. degrees in engineering applied mathematics from Hassan II University, Casablanca, Morocco, and Descartes University, Paris, France, in 2000 and 2001, respectively, the M.S. degree in statistics and signal processing from Pierre and Marie Curie University, Paris, in 2002, and the Ph.D. degree in signal processing and applied mathematics from Pierre and Marie Curie University, in collaboration with Telecom SudParis, France, in 2006. He was a Lecturer with the Paris-Dauphine and with the Vincennes-Saint-Denis Paris 8 University, in 2006 and 2007, respectively. He was a Postdoctoral Research Associate with the Superior School of electricity, Supelec, Paris, with the GIPAS-lab, Grenoble, France, with the Electrical Engineering Department, KFUPM, Saudi Arabia, and with the Spectral Analysis Laboratory, University of Florida, USA, in 2008, 2009, 2010, and 2011, respectively. He is currently working as an Associate Professor with the Electrical Engineering Department, Taif University, Saudi Arabia. His research interests are in the areas of statistical signal processing with application to the antenna array, radar application, and communication systems.

MOHAMED S. SOLIMAN (Senior Member, IEEE) received the Ph.D. degree in communications engineering from the Graduate School of Engineering, Osaka University, Japan. He is currently an Assistant Professor with the Department of Electrical Engineering, Faculty of Energy Engineering, Aswan University, Egypt. He is also with the Department of Electrical Engineering, Faculty of Engineering, Taif University, Saudi Arabia. His research interests include wireless communications, phased and timed array signal processing, UWB micro strip patch antennas, dielectric resonant antennas, numerical methods in electromagnetic, mimo antenna, optimization techniques in antenna design, and antenna measurement techniques. He is a Senior Member in IEEE-MTT/AP Society, KAUST chapter, Saudi Arabia.

YAHYA SALAMEH HASSAN KHRAISAT received the Dipl. Eng. M.Sc. degree in engineering from the Kiev Institute of Civil Aviation Engineers, Ukraine, in 1994, and the Ph.D. degree in engineering from the Kiev International University of Civil Aviation, Ukraine, in 1998. He was previously working as a Professor with the Electrical Engineering Department, Taif University, Saudi Arabia. He is currently working as a Full Professor with the Department of Electrical and Electronics Engineering, Al-Balqa' Applied University, Amman, Jordan. His research interests are in the areas of radar engineering with application to the antenna array, radar application, and cognitive radio systems.